Int. J. Electrochem. Sci., 10 **(2015)** 5981 - 5993

International Journal of
ELECTROCHEMICAL
SCIENCE
www.electrochemsci.org

Effects of Aluminum Addition on the High Temperature Oxidation Behavior of CM-247LC Ni-based Superalloy

Mau-Sheng Chiou[1], *Sheng-Rui Jian*[1,*], *An-Chou Yeh*[2], *Chen-Ming Kuo*[3]

[1] Department of Materials Science and Engineering, I-Shou University, Kaohsiung 840, Taiwan
[2] Department of Materials Science and Engineering, National Tsing Hua University, Hsinchu 300, Taiwan
[3] Department of Mechanical and Automation Engineering, I-Shou University, Kaohsiung 840, Taiwan
[*]E-mail: srjian@gmail.com

Received: 13 April 2015 / *Accepted:* 15 May 2015 / *Published:* 27 May 2015

The effects of adding 1 wt.% Al element on the oxidation behavior of CM-247LC Ni-based superalloy are studied under high temperature conditions, namely, 1000°C and 1150°C dry air isothermal oxidation test. The microstructure of oxides, γ matrix and γ′ precipitate are observed and analyzed by using X-ray diffraction (XRD) and scanning electron microscopy (SEM) techniques. Furthermore, the impacts of high temperature oxidation behavior and phase stability are realized. The results indicated that adding 1 wt.% Al could promote γ′ phase precipitate, which directly increases the volume fraction of γ′ phase in the substrate microstructure. Consequently, by adding 1 wt.% Al in CM-247LC Ni-based superalloys, the enhancement of Al activity and the formation of continuous Al_2O_3 protection layer to improve oxidation resistance are significantly promoted.

Keywords: Ni-based superalloys; Al; High-temperature oxidation; Microhardness.

1. INTRODUCTION

Ni-based superalloys, which have been developed and used in turbine engines since 1940's, show excellent high temperature strength and high temperature oxidation resistance [1-14]. Recently, the development of highly efficiency turbine engines pushes the turbine inlet temperature to a higher level, where the stringent temperature and hostile environment prompt the development of Ni-based superalloys especially in the aerospace applications. As turbine engine blades and vanes exposed to high temperature and gigantic thermal gradient, materials are susceptible to environmental attacks. Improving the high temperature oxidation resistance of Ni-based superalloys has always been a vital issue of alloy development [1, 2, 13, 15-17].

It is well known that Ni-based superalloys working under high temperature and hostile environment will yield oxides on the surface, such as Ta_2O_5, WO_3, TiO_2, Cr_2O_3 and Al_2O_3 [8, 10]. However, Al_2O_3 oxides can effectively obstruct the base material from further oxidation and reduce the rate of oxidation; therefore, the high temperature oxidation resistance can be improved [12-13]. In the previous studies [18-21], the high temperature oxidation resistance is improved enormously by adding a small amount of Al in the alloys. Since Al could stimulate the formation of Al_2O_3 and obstruct further oxidation, the high temperature capability of the alloys can be improved significantly by the addition of Al.

CM-247LC Ni-based superalloy was developed by Cannon-Muskegon Corporation (Michigan USA), which designed for both directionally solidified (DS) and conventional casting (CC) turbine blade and vane applications [15-18]. In the present study, the high temperature oxidation resistance can be expected to improve by the addition of 1 wt.% Al in CM-247LC. The phase stability of γ′ precipitates, γ matrix and the lattice misfit will be affected by varying the composition of superalloys. Therefore, the influence of adding Al in the microstructural properties and the oxidation behaviors of CM-247LC Ni-based superalloys are characterized by using X-ray diffraction (XRD), scanning electron microscopy (SEM) and back-scatted electron (BSE) techniques. In addition, the hardness of CM-247LC Ni-based superalloys is also measured by means of Micro Vickers indenter.

2. EXPERIMENTS

Table 1. Chemical compositions of specimens, in wt.%.

Alloy	Co	Al	Ti	Mo	W	Cr	Ta	Hf	B	Zr	C	Ni
CM-247LC	9.3	5.7	0.7	0.5	9.5	8.1	3.2	1.5	0.015	0.007	0.07	Bal.
CM-247LC with 1 wt.% Al addition	9.2	6.7	0.7	0.5	9.4	8	3.2	1.4	0.015	0.007	0.07	Bal.

CM-247LC polycrystalline superalloy was obtained from Cannon-Muskegon Co., and its nominal composition is listed in Table 1. By the use of vacuum arc remelting (VAR), alternative specimens with 1 wt.% Al addition were prepared; the compositions are also listed in Table 1. Two kinds of specimens were subjected to the same heat treatment schemes: solution treatment at 1260°C for 2 hour, argon cooling (AC) to ambient temperature, then first aging at 1079°C for 4 hour, AC; second aging at 871°C for 20 hour, AC. Specimens were prepared by diamond blade through precision cutter into cubic with 5 mm in length. The surfaces of each specimen were polished up to 800 grade sandpaper. By the use of box furnace, dry air isothermal oxidation tests were conducted at 1000°C and 1150°C, and test time were 1, 25, 100 and 175 hours. Heat treated specimens after oxidation tests were analyzed by PANalytical X'PERT PRO XRD. A Hitachi-4700 field-emission SEM equipped with a Horiba energy-dispersive X-ray spectrometry (EDS) system was used to observe and analyze the oxidation behavior and phase stability. BSE images were observed by a Hitachi-S3400N SEM. Micro Vickers indentations are made at the load of 10 g on the test samples using a hardness tester (Akashi MVK-H11).

3. RESULTS AND DISCUSSION

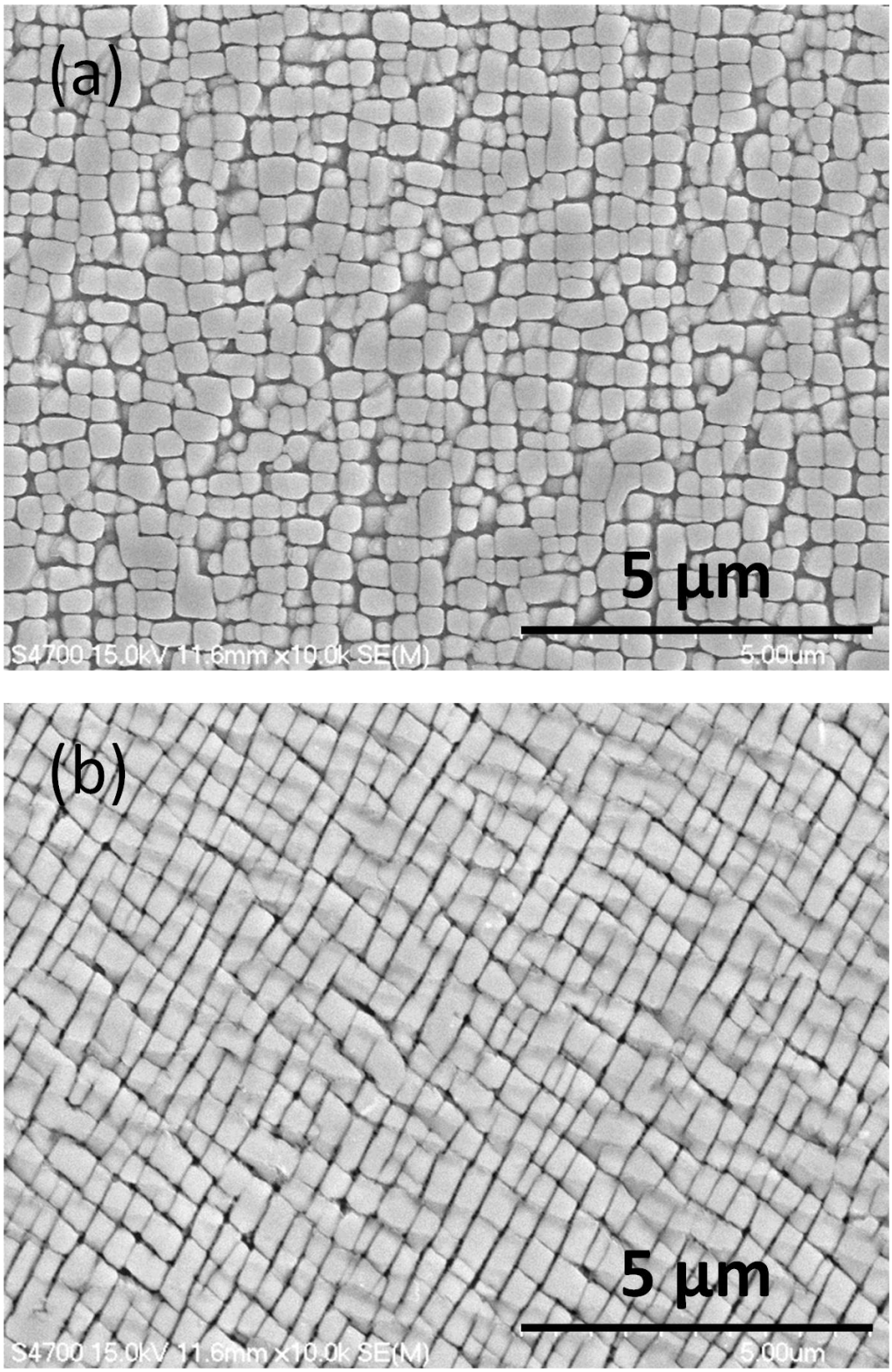

Figure 1. SEM micrographs of γ′ precipitates, (a) CM-247LC, (b) CM-247LC with 1 wt.% Al addition.

In this work, both CM-247LC and with 1 wt.% Al addition alloys were polycrystalline. Since the grain size is similar subjected to heat treatment, influences of grain boundaries are not discussed. The SEM photographs of both CM-247LC and with 1 wt.% Al addition alloys after heat treatment processes are shown in Fig. 1. The average size of γ′ precipitates was about 500 nm for both alloys, whereas γ channel width of CM-247LC with 1 wt.% Al addition specimen was smaller than that of CM-247LC specimen. Because the addition of Al could promote γ′ precipitate, the γ′ volume fractions of CM-247LC and with 1 wt.% Al addition are 70% and 77%, respectively. The elemental partitioning characteristics between γ and γ′ of CM-247LC have been proposed by Yeh *et al*. [22].

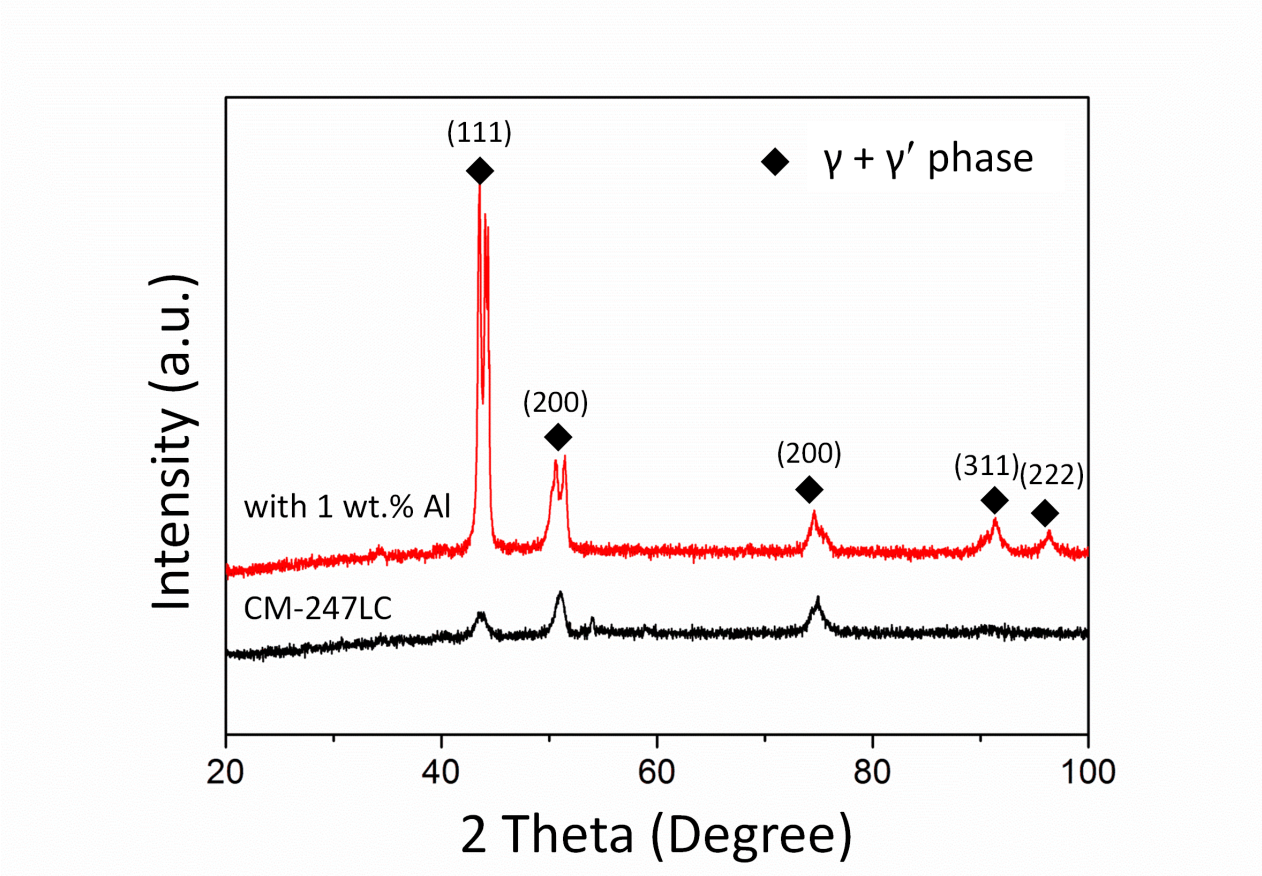

Figure 2. XRD pattern of CM-247LC and CM-247LC with 1 wt.% Al addition base materials.

XRD patterns of both CM-247LC and with 1 wt.% Al addition alloys after full heat treatment are shown in Fig. 2. Result shows the peak intensity of γ + γ′ phase of CM-247LC with 1 wt.% Al addition was better than CM-247LC in each lattice planes. The lattice misfit (δ) is well defined by the following equation [4, 22-23],

$$\delta = \frac{2(a_{\gamma'} - a_{\gamma})}{a_{\gamma'} + a_{\gamma}} \quad (1)$$

where $a_{\gamma'}$ and a_{γ} are the lattice parameters of γ′ and γ phases, respectively. The lattice parameters of each lattice plane and corresponding lattice misfit of both alloys are listed in Table 2. The misfit values

of both alloys are negative. The effect of Al addition exhibits much larger lattice misfit toward negative than regular CM-247LC, and promote microstructural instability. Thus, by adding 1 wt.% Al in CM-247LC, the γ′ phase precipitate is promoted and the volume fraction of γ′ phase is increased, and further leading the γ channel to narrow.

Table 2. Lattice parameters of γ and γ′ phases as well as constrained lattice misfit of CM-247LC and CM-247LC with 1 wt.% Al addition alloys.

Alloy	lattice plane	a_γ (Å)	$a_{\gamma'}$ (Å)	Lattice misfit δ
CM-247LC	(111)	3.6	3.568	-0.89%
	(200)	3.594	3.563	-0.86%
CM-247LC with 1 wt.% Al addition	(111)	3.595	3.536	-1.65%
	(200)	3.607	3.547	-1.68%

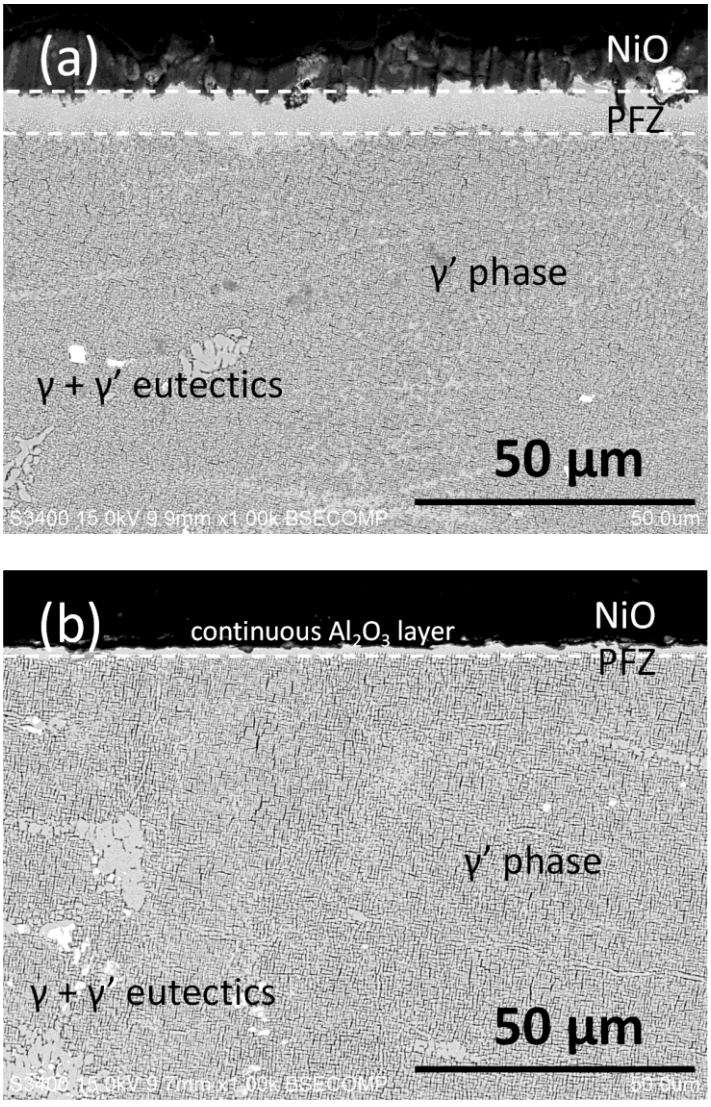

Figure 3. BSE images after 1 hour dry air isothermal oxidation at 1000°C: (a) CM-247LC, (b) CM-247LC with 1 wt.% Al addition.

The cross-sectional microstructures of CM-247LC and with 1 wt.% Al addition specimens subjected to 1 hour dry air isothermal oxidation at 1000^{o}C are shown in Fig. 3(a) and Fig. 3(b), respectively. In Fig. 3, an oxide layer (mainly NiO) was grown on the surface and a layer of γ′ precipitate-free zone (PFZ) was generated between the NiO oxide layer and the matrix. It can be seen that the thickness of NiO oxide layer and PFZ layer are increased by 50% without adding Al during high temperature oxidation, suggesting that the oxidation behavior is seriously, as compared with Fig. 3(a) and Fig. 3(b). Therefore, a continuous Al_2O_3 layer is formed rapidly to protect the oxidation of matrix and further improve its oxidation resistance effectively by addition of 1 wt.% Al in CM-247LC Ni-based superalloy.

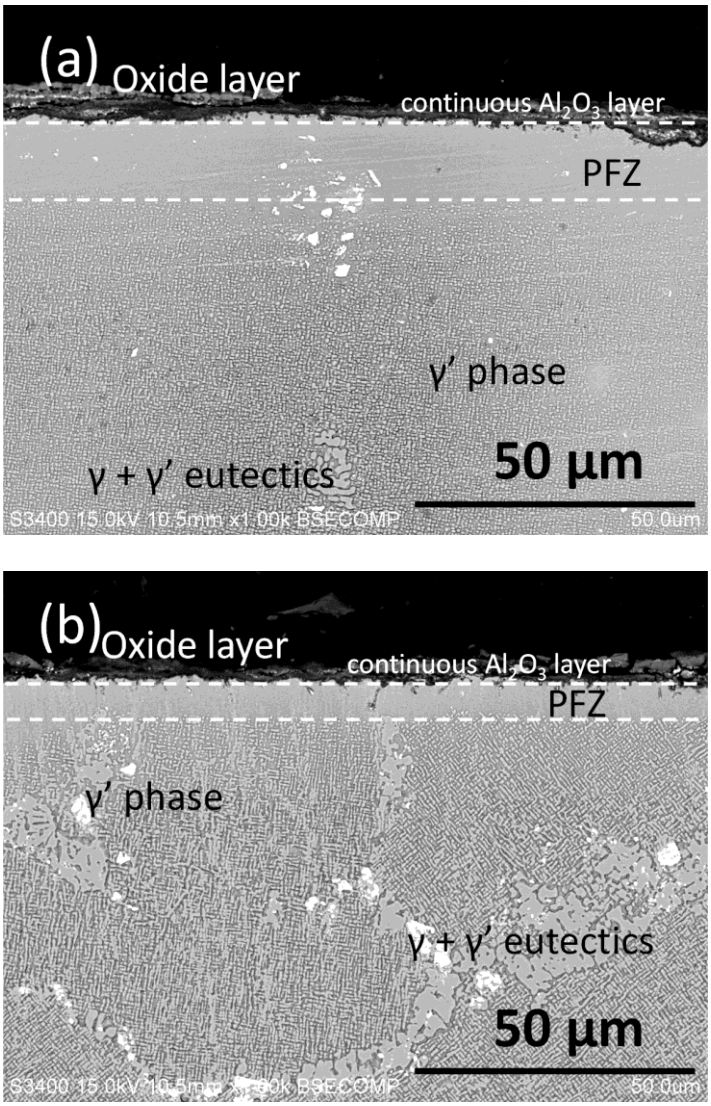

Figure 4. BSE images subjected to dry air isothermal oxidation process at 1150^{o}C at the oxidation time of 1 hour: (a) CM-247LC, (b) CM-247LC with 1 wt.% Al addition.

The oxide layers in Fig. 4 not only consist of NiO, but also WO_3 and Co_3O_4 mixed on the top surfaces of both CM-247LC and with 1 wt.% Al addition specimens after 1 hour dry air isothermal oxidation test at 1150^{o}C. As shown in Fig. 4(a), the continuous Al_2O_3 layer is formed in CM-247LC

specimens subjected to 1 hour oxidation treatment at 1150^{o}C, which is not found in Fig. 3(a). In addition, the PFZ layer of CM-247LC is also much thicker than that of CM-247LC with 1 wt.% Al addition specimen.

As Ni-Cr-Al system alloys at stable state, oxides are constituted from different types due to multiple components. The compositions of CM-247LC alloys have little Cr and Al contents; causing the NiO layers are formed subjected to 1 hour oxidation process at 1000^{o}C. The Cr element is easy to form Cr_2O_3 and provide good oxidation resistance at high temperature. The Cr_2O_3 can be reactive (1/2 Cr_2O_3 + 3/4 O_2 = $CrO_{3(g)}$) to form CrO_3 volatile phase under high oxygen partial pressure and high temperature (T > 1000^{o}C) [24-25]; thus, the Cr_2O_3 oxide layer is not observed here. Consequently, by adding 1 wt.% Al can enhance the Al activity, thermodynamically stable Al_2O_3 and enhance the matrix oxidation resistance.

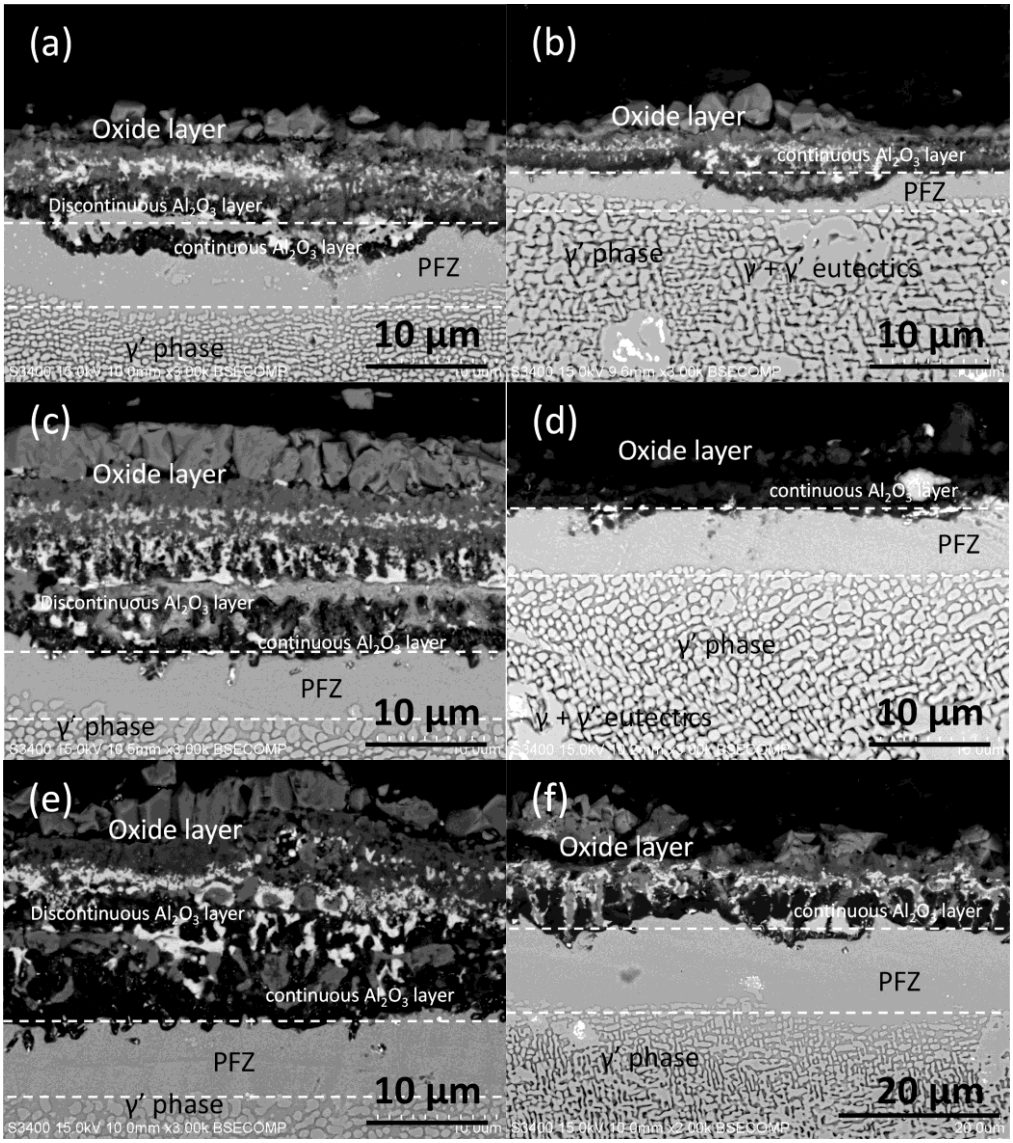

Figure 5. The cross-sectional BSE images in CM-247LC: (a) 25 hours, (c) 100 hours, (e) 175 hours; CM-247LC with 1wt.% Al addition: (b) 25 hours, (d) 100 hours, (f) 175 hours, subjected to dry air isothermal oxidation process at 1000^{o}C.

The cross-sectional BSE images of dry air isothermal oxidation at 1000°C treated CM-247LC and with 1 wt.% Al addition specimens at the various oxidation time of 25, 100 and 175 hours are shown in Fig. 5, respectively. It can be seen that the oxide layer on the surface of CM-247LC is become thicker without Al addition. And, the discontinuous Al_2O_3 layer is generated between oxide layer and continuous Al_2O_3 layer. With increasing the oxidation time, the Al_2O_3 protection layer cannot provides enough protection to the matrix, indicating that the internal oxidation is occurring. On the contrary, CM-247LC with 1 wt.% Al addition specimen seems to be affected slightly only after 175 hour. Therefore, internal oxidation happened in CM-247LC was much more serious than that of CM-247LC with 1 wt.% Al addition. It was known that Al_2O_3 layer can prevent cation diffusion outward and oxygen ions diffusion inward effectively [24-25]. Therefore, the formation of continuous Al_2O_3 layer can be promoted by adding Al in CM-247LC alloys.

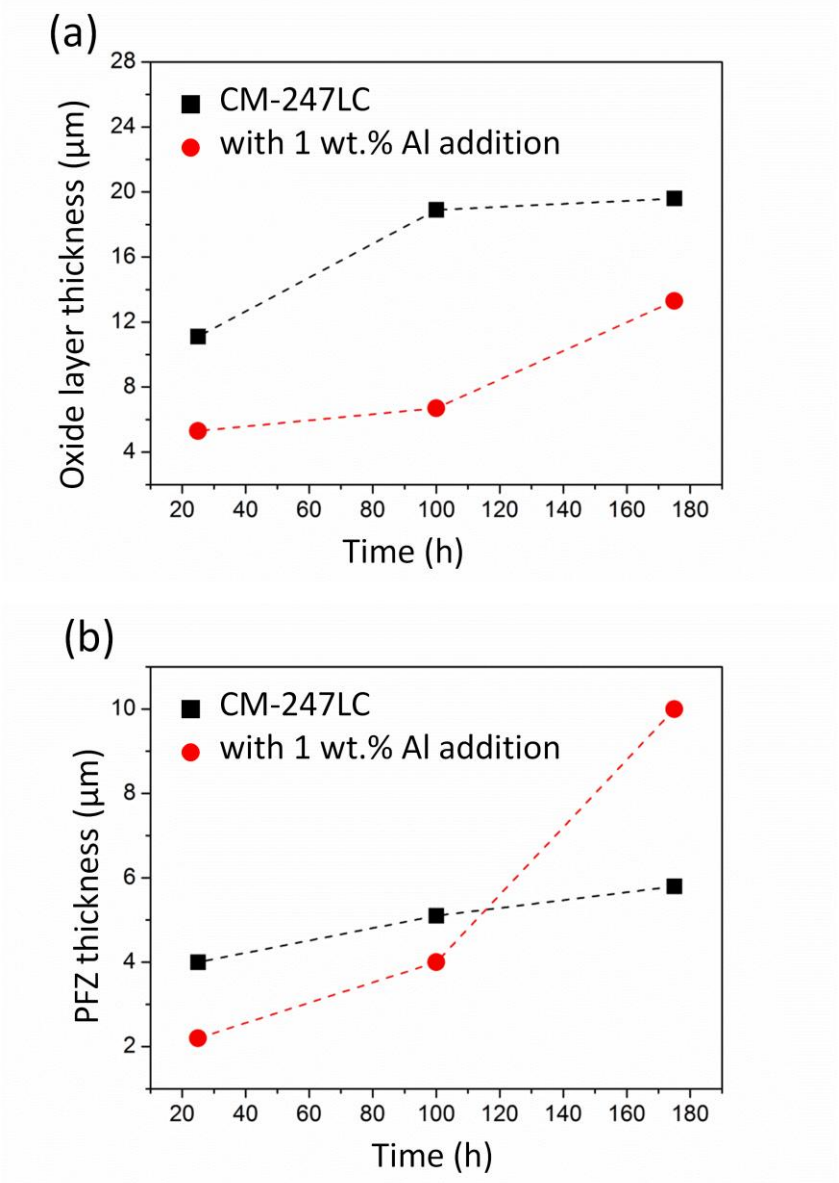

Figure 6. The thickness of (a) Oxide layer and (b) PFZ for CM-247LC and with 1 wt.% Al addition specimens subjected to dry air isothermal oxidation process at 1000°C with the various oxidation time.

The thickness of oxide layer for CM-247LC and with 1 wt.% Al addition specimens subjected to at 1000°C dry air isothermal oxidation process with the various oxidation time are shown in Fig. 6(a) and Fig. 6(b). With increasing the oxidation time, the oxide layer and PFZ become thick in both cases. The Al_2O_3 layer and PFZ are observed thicker in the addition of 1wt.% Al CM-247LC alloy, indicating that Al element is promoted to form the continuous Al_2O_3 layer rapidly to obstruct the interdiffusion and, simultaneously, the thicker PFZ layer is generated due to the diffusion of Al from γ' (Ni_3Al) phase during high temperature oxidation process.

According to the parabolic rate law of oxidation [12],

$$d^2 = k_p t \tag{2}$$

where d is oxide layer thickness, k_p is the parabolic oxidation rate constant, and t is the exposure time. The linear curve fit of oxidation parabolic rate law for both CM-247LC and with 1 wt.% Al addition specimens subjected to dry air isothermal oxidation process at 1000°C is shown in Fig. 7. The parabolic oxidation rate constant k_p of both CM-247LC and with 1 wt.% Al addition specimens are 4.86×10^{-4} μm^2/s and 2.75×10^{-4} μm^2/s, respectively. The k_p value of CM-247LC with 1 wt.% Al addition is smaller than that CM-247LC, suggesting that adding Al element in CM-247LC could reduce the oxidation rate significantly.

The cross-sectional BSE images of dry air isothermal oxidation at 1150°C treated CM-247LC and with 1 wt.% Al addition specimens at the various oxidation time of 25, 100 and 175 hours are shown in Fig. 8, respectively. Compared with Fig. 5, as the oxidation temperature is raised to 1150°C, it becomes clear that the several pores have already generated and occupied the PFZ and matrix, as shown in Figs. 8(a), 8(c) and 8(e). However, there are no pores observed in the matrix; such events observed here are conceived to intimately relate to the addition of Al. Consequently, even at the higher temperature (1150°C), the matrix is still remained with the aid of the Al addition during high temperature oxidation processes, as shown in Figs. 8(b), 8(d) and 8(f).

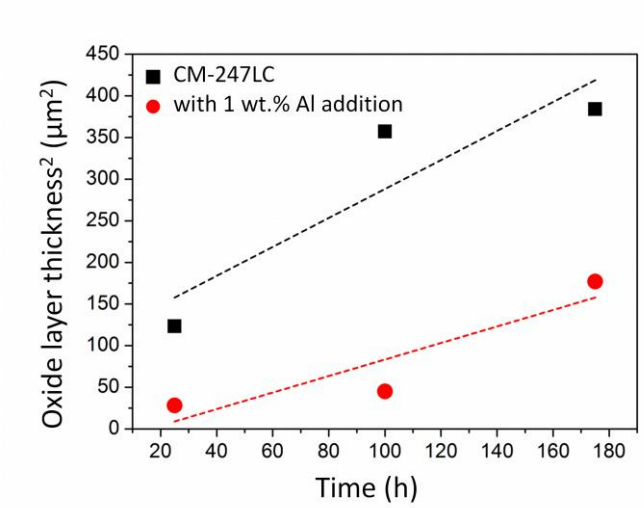

Figure 7. The linear curve fit of oxidation parabolic rate law for CM-247LC and with 1 wt.% Al addition specimens subjected to dry air isothermal oxidation process at 1000°C.

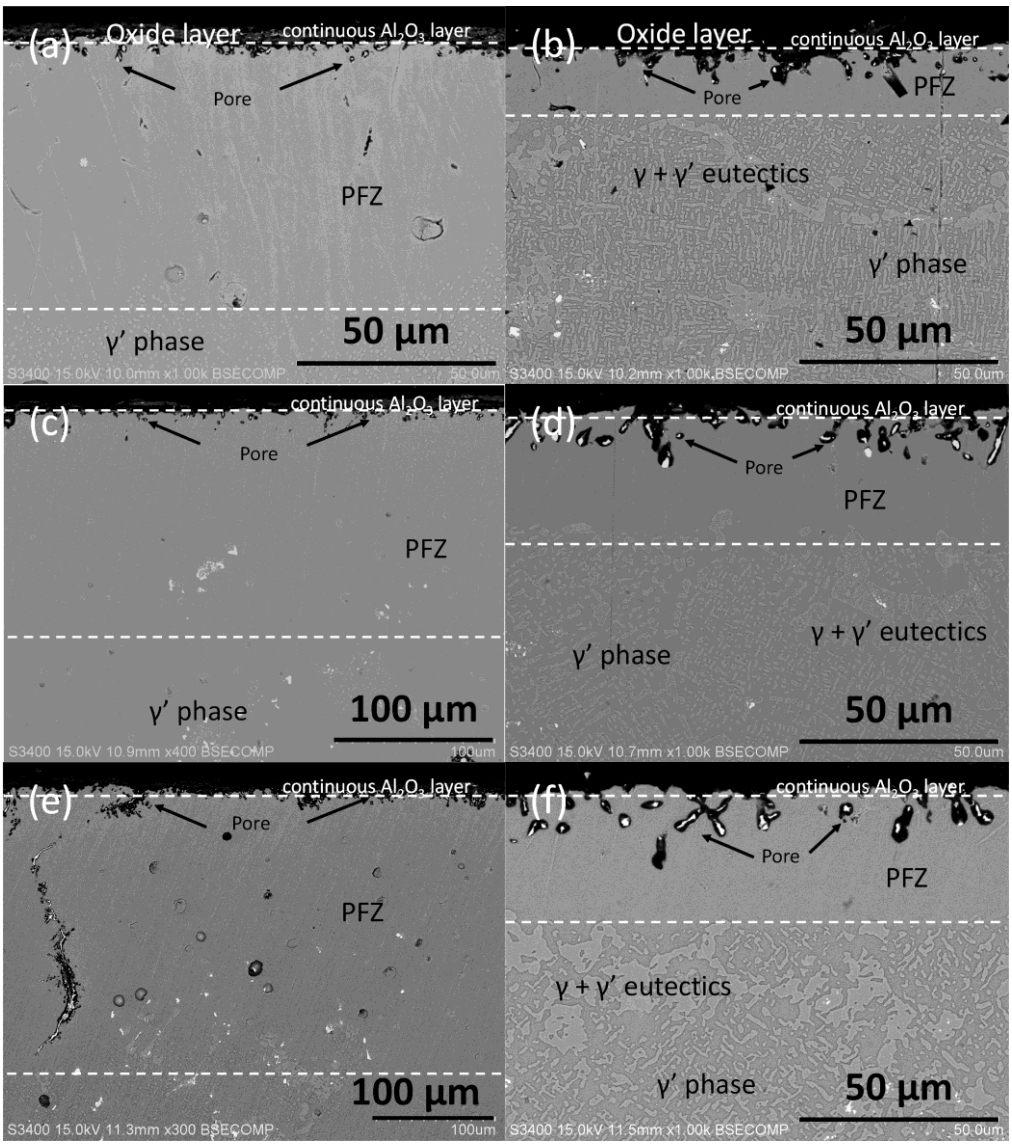

Figure 8. The cross-sectional BSE images in CM-247LC: (a) 25 hours, (c) 100 hours, (e) 175 hours; CM-247LC with 1wt.% Al addition: (b) 25 hours, (d) 100 hours, (f) 175 hours, subjected to dry air isothermal oxidation process at 1150^{o}C.

Table 3. The average microhardness values of CM-247LC and with 1 wt.% Al addition specimens subjected to 175 hour dry air isothermal oxidation process at 1000^{o}C.

	CM-247LC	CM-247LC with 1 wt.% Al addition
Base material	431.4±15.8 Hv	516.9±12.4 Hv
PFZ	316.7±7.4 Hv	316.6±13.5 Hv

Micro Vickers indentation measurements are used to measure the CM-247LC and with 1wt.% Al addition specimens subjected to 175 hour oxidation treatment at 1150^{o}C. Since the oxide layer is very complex, non-uniform and easy to peel off, hardness test is only performed at PFZ and base

material. SEM micrographs of indentations are shown in Fig. 9, where no cracking events around the indentation are observed. The average hardness values of both CM-247LC and with 1 wt.% Al addition are shown in Table 3. The microhardness value of CM-247LC with 1 wt.% Al addition is larger than that CM-247LC. It is known that adding 1wt.% Al could promote γ′ phase precipitate, increase the volume fraction of γ′ phase and then improve the strength of matrix. In addition, the microhardness values of PFZ for CM-247LC and with 1 wt.% Al addition are similarly. Because some elements diffused away from γ′ phase to the surface and formed oxides on the surface, the chemical composition of PFZ is approximately pure Ni. Therefore, the microhardness values of PFZ for two samples have no manifestly difference.

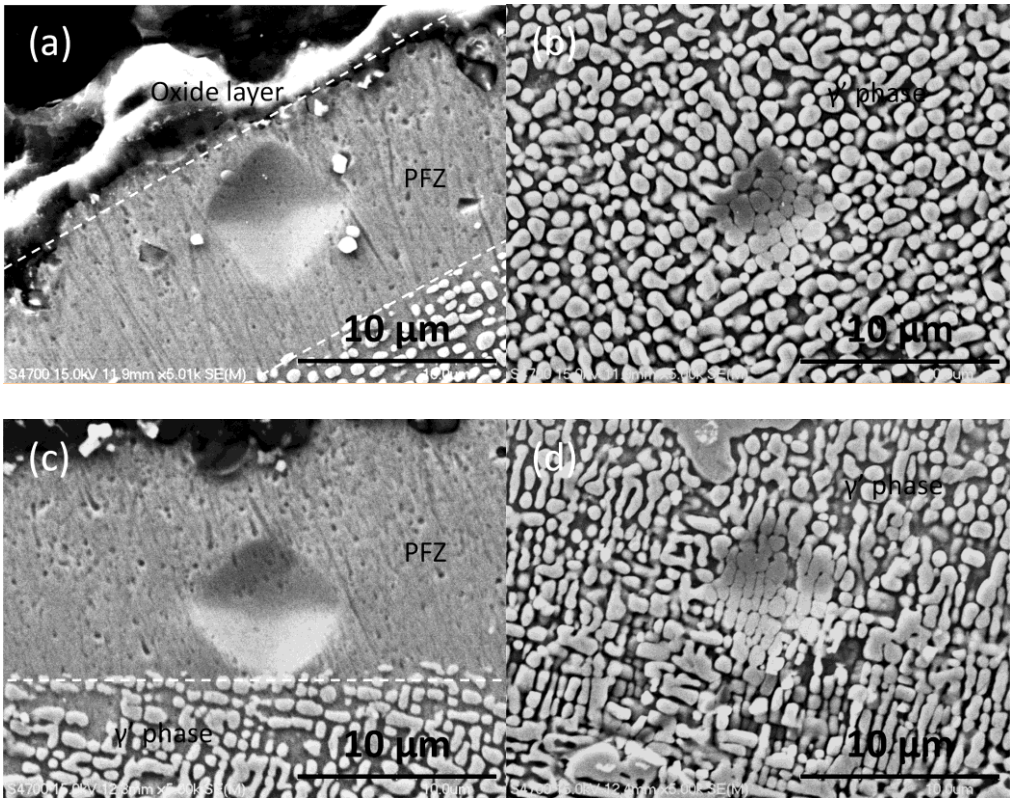

Figure 9. SEM micrographs of Micro Vickers indentation subjected to 1000 ^{o}C dry air isothermal oxidation at the oxidation time of 175 hour: (a) CM-247LC PFZ, (b) CM-247LC base material, (c) CM-247LC with 1wt.% Al addition PFZ, and (d) CM-247LC with 1wt.% Al addition base material.

4. CONCLUSIONS

In conclusion, the effects of Al addition on the microstructural properties of the oxidation behaviors of CM-247LC Ni-based superalloys could be summarized as followings:

1. The addition of Al in CM-247LC superalloys could cause elemental partitioning characteristics toward γ′ and promote γ′ phase precipitation, increasing the volume fraction of γ′ phase and further causing the lattice misfit between γ′ and γ phases more negative. Increasing the γ′ phase volume fraction could also improve the strength of base material.

2. Al addition also enhances Al activity and promotes the formation of continuous Al_2O_3 protection layer to improve oxidation resistance.
3. CM-247LC Ni-based superalloy is commercially available in the turbine engine business. Small variation in Al content could significantly influence its oxidation behavior.
4. The microhardness values of CM-247LC Ni-based superalloy is enhanced about 20% by the addition of 1 wt.% Al.

ACKNOWLEDGEMENT
This work was supported by Ministry of Science and Technology under grant numbers NSC 100-2632-E-214-073-MY3 and MOST 103-2221-E-214-035. X-ray, SEM and BSE photographs were conducted at MANA-Laboratory of I-Shou University. Authors like to thank Ms. Ya-Yun Lin for her technical supports.

References

1. I. Gurrappa, *Oxidation of Metals*, 51 (1999) 353-382.
2. F.H. Yuan, Y.S. Yoo, C.Y. Jo, B.G. Choi, and Z.Q. Hu, *Surface and Coatings Technology*, 183 (2004) 106-110.
3. S. Sinharoy, and S.L. Narasimhan, *Superalloys*, U.S.A. (2004) 623-626.
4. S. Ma, D. Brown, M.A.M. Bourke, M.R. Daymond, and B.S. Majumdar, *Materials Science and Engineering* A, 399 (2005) 141-153.
5. H. Wei, G.C. Hou, X.F. Sun, H.R. Guan, and Z.Q. Hu, *Oxidation of Metals*, 68 (2007) 149-163.
6. A.C. Yeh, K. Kawagishi, H. Harada, T. Yokokawa, Y. Koizumi, T. Kobayashi, D.H. Ping, J.Fujioka, and T. Suzuki, *Superalloys*, U.S.A. (2008) 619-628.
7. C.M. Kuo, Y.T. Yang, H.Y. Bor, C.N. Wei, and C.C. Tai, *Materials Science and Engineering* A, 510 (2009) 289-294.
8. A. sato, Y.L. Chiu, and R.C. Reed, *Acta Materialia*, 59 (2011) 225-240.
9. B. Bai, H. Guo, H. Peng, L. Peng, and S. Gong, *Corrosion Science*, 53 (2011) 2721-2727.
10. I.V.S. Yashwanth, I. Gurrappa, and H. Murakami, *Journal of Surface Engineered Materials and Advanced Technology*, 1 (2011) 130-135.
11. A.C. Yeh, K.W. Lu, C.M. Kuo, H.Y. Bor, and C.N. Wei, *Materials Science and Engineering* A, 530 (2011) 525-529.
12. M. Bensch, A. Sato, N. Warnken, E. Affeldt, R.C. Reed, and U. Glatzel, *Acta Materialia*, 60 (2012) 5468-5480.
13. K. Kawagishi, A.C. Yeh, T. Yokawa, T. Kobayashi, Y. Koizumi, and H. Harada, *Superalloys*, U.S.A. (2012) 189-195.
14. D.K. Das, *Progress in Materials Science*, 58 (2013) 151-182.
15. H.E. Huand, and C.H. Koo, *Materials Transactions*, 2 (2004) 562-568.
16. I.S. Kim, B.G. Choi, S.M. Seo, D.H. Kim, and C.Y. Jo, *Materials Letters*, 62 (2008) 1110-1113.
17. M.Z. Alam, D.V.V. Satyanarayana, D. Chatterjee, R. Sarkar, and D.K. Das, *Materials Science and Engineering* A, 536 (2012) 14-23.
18. M.Z. Alam, D. Chatterjee, B. Venkataraman, V.K. Varma, and D. Das, *Materials Science and Engineering* A, 527 (2010) 6211-6218.
19. K.L. Lin, and T.P. Liu, *Oxidation of Metals*, 50 (1998) 255-267.
20. D. Mudgal, S. Singh, and S. Prakash, *Journal of Minerals & Materials Characterization & Engineering*, 11 (2012) 211-219.
21. O.P. Gupta, D. Mudgal, D. Puri, and S. Prakash, *International Journal of Advanced Scientific Research and Technology*, 2 (2012) 486-492.
22. A.C. Yeh, K.C. Yang, J.W. Yeh, C.M. Kuo, *Journal of Alloys and Compounds*, 585 (2014) 614-621.

23. X. Li, X.N. Zhang, C.P. Liu, C.Y. Wang, T. Yu, and Z. Zhang, *Journal of Alloys and Compounds*, 633 (2015) 366-369.
24. J. Huang, H. Fang, X. Fu, F. Huang, H. Wan, Q. Zhang, S. Deng, and J. Zu, *Oxidation of Metals*, 53 (2000) 273-287.
25. M.H. Li, X.F. Sun, T. Jin, H.R. Guan, and Z.Q. Hu, *Oxidation of Metals*, 60 (2003) 195-210.